Enhanced field emission of electrons from wrinkled graphene: A unified approach

Sylvester W. Makumi,[1,†] Stefanie Haugg,[2,†] Bojan Bosnjak,[2] Robert Zierold,[2] Robert H. Blick,[2] and Zlatan Aksamija[1,*]

[1] *Department of Materials Science and Engineering, University of Utah, Salt Lake City, Utah, USA*
[2] *Center for Hybrid Nanostructures, Universität Hamburg, Hamburg, Germany*

(Received 25 December 2023; revised 22 March 2024; accepted 17 July 2024; published 8 August 2024)

Field emission (FE), the process of emitting electrons from the surface of a metal under large perpendicular electric fields, has a long history and plays a crucial role in numerous applications ranging from electron microscopes to detectors. A key determining factor for FE is the work function of the material. Graphene is semimetallic and has a work function that can be tuned by the position of the Fermi level, lending it a distinct advantage in FE applications. However, the exceptional thinness of graphene means its properties are highly dependent on the environment and the substrate that it is supported on. The impact of environmental factors, particularly the atomic-scale roughness of the substrate to which graphene typically conforms, on FE has not been explored. Here, we demonstrate that atomic-scale roughness dictates FE currents by controlling the local slope of the graphene sheet relative to the electric field. Our study combines measurements of FE current from graphene supported over trenches and supported on silicon nitride substrates, while our calculations capture the full electronic structure from first principles and model the adhesion of graphene to a rough substrate via van der Waals forces. Our results show that the FE current scales with the average slope of the substrate's surface, which, in turn, depends on the ratio of roughness and correlation length of the atomic-scale roughness. This novel relationship explains our observation that FE currents are larger from supported graphene samples compared with those suspended over micron-scale trenches. Our work impacts future applications of graphene in FE by allowing researchers to maximize the FE current through surface engineering.

DOI: 10.1103/PhysRevApplied.22.024022

I. INTRODUCTION

Graphene, a two-dimensional (2D) allotrope of carbon, has been the subject of intense study over the past two decades. While its superlative mechanical [1], electronic [2], and thermal [3,4] properties have received widespread attention, graphene continues to surprise us with unique phenomena, opening new doors into 2D physics. One such unique property of graphene is its tunable work function (WF)—because graphene is semimetallic, its WF can be varied over a wide range of 4.5–4.8 eV by modifying the charge carrier concentration using an external electric field [5] and further lowered by surface modification [6]. The variable WF, coupled with graphene's thinness and mechanical strength, opens up a host of potential applications for graphene in field emission (FE) as well as thermionic emission (TE) [7], which may be useful in a variety of energy and sensing applications.

Several studies considered the FE properties of graphene and demonstrated that stable FE can be obtained [8] but with most of the current originating from edges and wrinkles [9] rather than the flat portion of the graphene flake [10]. The measured FE current followed a modified Fowler-Nordheim (FN) law [11,12] owing to the unique electronic structure of graphene composed of Dirac cones with nearly linear dispersion [12]. Another widely known property of graphene is its tendency to wrinkle, both when it is suspended and when it is supported on a substrate [13]. Atomic-scale surface roughness of the substrate can induce wrinkles as graphene partially conforms to the surface of the substrate, with a typical corrugation height of 1 nm and length scale of 15 nm [14]. Graphene supported on an array of InP nanocrystals has also been shown to enhance field emission [15]. However, the impact of wrinkling and local curvature of suspended and supported graphene on its FE properties has not yet been elucidated.

Here, we study FE from monolayer graphene samples on both intentionally patterned and macroscopically flat but atomically rough substrates. Our hypothesis is that FE can be increased by bending the graphene sheet to decrease the angle between the sheet and the electric field. To test this hypothesis, we measure the FE current as a function of the applied electric field and show that, in accordance with

*Contact author: zlatan.aksamija@utah.edu
†These authors contributed equally

our hypothesis, FE current from graphene suspended over wide and deep trenches in the substrate is lower than that from graphene suspended over narrow trenches. However, FE current from graphene on an atomically rough substrate was even higher.

To analyze the experimental results, we develop a generalized theory of field and thermionic emission from wrinkled graphene based on the first-principles electronic structure of graphene and a numerical model for corrugation due to graphene partially conforming to the atomically rough substrate. Our calculations show that FE depends on the angle between the graphene surface and the electric field because the electron supply is a function of the cosine of the angle between the electron velocity and the field, which are perpendicular in flat graphene. Using this concept, we demonstrate that atomic-scale roughness causes graphene to tilt locally and can produce larger angles than graphene draped over trenches, thus explaining the larger FE from graphene on a macroscopically flat substrate. We conclude that intentionally roughening the surface of the substrate prior to the transfer of graphene is a promising avenue toward further enhancing FE. Our results may pave the way for realistic applications of graphene as a field emitter on a variety of substrates engineered for optimal performance.

II. METHODOLOGY

A. Calculations of field-emission current

To understand the field emission from graphene on a variety of nonflat and patterned substrates, we develop a comprehensive numerical simulation of field emission from graphene. Without any loss of generality, we assume that the graphene's lateral dimensions are infinite and the electric field is uniform across it, pointing in the z-direction. In the most general case, the graphene sheet can be locally tilted from the vertical by an angle θ, with a $\pi/2$ angle meaning the graphene is flat with respect to the x–y plane and perpendicular to the electric field. We denote the axis in the x–y plane around which the graphene sheet is tilted as having an angle ϕ from the x-axis. The magnitude of the electron velocity inside the graphene sheet is approximately equal to the Fermi velocity v_{F}; however, this velocity is then decomposed into components along the field and perpendicular to the field $v_\perp$. Therefore, the perpendicular velocity with which electrons attempt to escape the surface of graphene is $v_\perp = v_F(k_z/|\vec{k}|) = v_F\cos(\theta)\sin(\phi)$. Averaging this over the angle ϕ in the x–y plane and considering that only electrons with a positive $v_\perp$ contribute to the FE current, we have the angular average $v_\perp = v_F\cos(\theta)/\pi$. The total kinetic energy of electrons in the graphene sheet is unaffected by the tilt as all the kinetic energy is completely contained in the sheet, but we can decompose the electron momentum into perpendicular and in-plane components analogous to the velocity. Then, $\hbar k_\perp = \hbar|\vec{k}|\cos(\theta)$ and the kinetic energy of the free electron, once emitted from the surface of graphene, would be $E_\perp(\vec{k}) = (\hbar^2k^2\cos^2\theta)/2m$ [12].

The FE current is obtained by integrating the product of the transmission probability at each $E_\perp$ and the number of electrons per area per unit of time attempting to emit, sometimes called the supply function $N(E_\perp)$, over all perpendicular energies [11] so that

$$J(T,F) = q\int_0^\infty T_{\mathrm{FE}}(E_\perp,F)N(E_\perp,T)dE_\perp, \tag{1}$$

where q is the electron charge, T is the temperature, and F is the applied electric field. The transmission probability is calculated in the WKB approximation [16], as elaborated in Supplemental Material, Sec. S1 and Eq. (S1) [17]. The supply function is obtained by integrating over all the available states. Following Liang and Ang [18], we express the supply function as

$$N(E_\perp,T)dE_\perp = \frac{\cos(\theta)}{\pi}\,dE_\perp\int_{E_\perp}^\infty v(E-E_\perp)g(E-E_\perp)f_{\mathrm{FD}}(E,T)dE, \tag{2}$$

where $f_{\mathrm{FD}}(E,T) = \{1+\exp[(E-E_F)/k_BT]\}^{-1}$ is the Fermi-Dirac distribution function. However, our supply function contains a term $\cos|\theta|$ from the perpendicular component of electron velocity, so the entire FE current density is then also proportional to $\cos|\theta|$, meaning that

$$J(T,F,\theta) = \frac{q\cos(\theta)}{\pi}\int_0^\infty T_{\mathrm{FE}}(E_\perp,F)\left[\int_{E_\perp}^\infty v(E-E_\perp)g(E-E_\perp)f_{\mathrm{FD}}(E,T)dE\right]dE_\perp. \tag{3}$$

Here, an angle of 0 would mean that the sheet is directed along the field and the result of ref. [8] is recovered.

Consequently, we can factor the current into two terms, one that has the angle dependence and another that contains the field dependence. For a corrugated or wrinkled sheet, the angle θ will vary with position, as discussed in the following section. Then, we can write the total current as the integral over the area to obtain

$$J(T,F) = \frac{1}{A}\int dx\,dy\,J(T,F,\theta)$$
$$= J(T,F,0)\int dx\,dy\,\cos[\theta(x,y)]$$
$$= J(T,F,0)\,\langle\cos(\theta)\rangle\,. \quad (4)$$

Here, A represents the area of the sheet while $\langle . \rangle$ stands for the average over the whole surface.

Electrons near the Dirac point within the graphene sheet are typically described by the massless Dirac equation $-v_F\hbar\vec{\sigma}\cdot\vec{\nabla}\psi(x,y) + U(x,y)\psi(x,y) = E\psi(x,y)$, while the electrons in vacuum after leaving the graphene sheet are treated as free electrons. The energy of electrons near the Dirac point in graphene can be approximated as $E(\vec{k}) = \pm\hbar v_F|\vec{k}| = \pm\hbar v_F\sqrt{k_x^2 + k_y^2}$ for a planar sheet in the x–y plane and the density of states (DOS) is linear in energy so that

$$g(E) = \frac{2}{\pi\hbar^2 v_F^2}|E|.$$

As shown by Ang *et al*. [19], the contribution from electrons with energies more than 1 eV above the Dirac point can be severely underestimated by the linear cone model [Eq. (1)]. To avoid this limitation and go beyond prior work, we calculate the electronic structure of graphene from first principles using the open-source density functional theory (DFT) code known as QUANTUM ESPRESSO [20]. We also compute the electron group velocities from the gradients of the electronic structure as

$$\vec{v}(\vec{k}) = \frac{1}{\hbar}\nabla_{\vec{k}}E_{\vec{k}},$$

and obtain the DOS from it numerically as

$$v(E)g(E)dE = \frac{dE}{(2\pi)^2}\iint d^2k\;\vec{v}(\vec{k})\delta(E - E_{\vec{k}})$$
$$= \frac{dE_\perp}{(2\pi)^2}\oint_{E=E_k}\frac{v(k)dl}{|\nabla_k E_k|}, \quad (5)$$

where the integration over the constant energy contour is performed by employing a 2D version of the spherical averaging (SAVE) numerical method [21]. Briefly, in this method, we linearly expand the energy around each discretization point k_i using its gradient $E(\vec{k}) \approx E(k_i) + (\vec{k} - k_i)\nabla_{\vec{k}}E(\vec{k})$ inside a small circle of radius R in momentum space. Then, the constant energy contour at some energy value E is perpendicular to the gradient inside this circle and has a length $L_i(E) = 2\sqrt{R^2 - (\vec{k} - k_i)^2}$, where the distance $\vec{k} - k_i = [E - E(k_i)]/|\nabla_{\vec{k}}E(k_i)|$. The electronic structure computed from DFT is plotted in Fig. S1 (see Supplemental Material [17]) along with the resulting DOS.

B. Calculations of graphene wrinkling and slope

Our model shows that there is no emission from an idealized, completely flat graphene sheet because the $\cos(\theta)$ term suppresses contributions from electrons with zero out-of-plane velocity ($\theta = \pi/2$). In such a case, electrons have zero kinetic energy in the perpendicular direction (along the field), which, in turn, makes the supply function hit zero. This situation has been considered in the literature [22], where FE from a perfectly flat graphene sheet was treated using a different approach based on phonon-assisted emission. However, even suspended graphene is never perfectly flat as lattice vibrations cause small local wrinkling and bending, and rough surfaces have been shown to impact FE [23]. Furthermore, carrier scattering by inhomogeneities can also relax the conservation of in-plane momentum, allowing emission [24,25]. Experiments have shown that the FE from the flat part of graphene sheet is indeed small [10] compared with the edges and creases, which is corroborated by our data, and that significant wrinkling exists in both suspended [26] and supported graphene [27].

Graphene is typically supported on a substrate and the surface of that substrate will have some atomic-scale roughness. Graphene conforms to that roughness, at least partially, following the crevices in the surface unless they are too steep, such as when the rms roughness is large or the surface has low correlation length, and the graphene delaminates from the substrate instead of draping over the large crevices in the substrate. To capture the emission from graphene on a rough substrate, we first generate the surface profile given a rms roughness $\Delta_{\rm rms}$ and correlation length $L_{\rm cor}$ using an algorithm based on the inverse fast Fourier transform (IFFT) [28]. This approach starts with a Fourier transform of the surface height autocorrelation function, which we take to be exponential $C(\vec{r}) = \langle h(\vec{r}')h(\vec{r}' - \vec{r}\rangle = \Delta_{\rm rms}^2\exp\left[-\sqrt{2}|\vec{r}|/L_{\rm cor}\right]$, to obtain the squared power spectrum $|S(\vec{q})|^2 = \mathcal{F}[C(\vec{r})]$. We then perform an IFFT after randomizing the phase φ to attain the surface height $h(\vec{r}) = \mathcal{F}^{-1}[S(\vec{q})e^{i\varphi}]$ [29]. The resulting surface height is randomized but with rms roughness $\Delta_{\rm rms}$ and correlation length $L_{\rm cor}$.

After generating the surface, we proceed to minimize the total energy of the graphene sheet on this rough surface. We calculate the total energy by adding together the van der Waals (vdW) adhesion energy $U_{\rm vdW}$, flexural energy $U_{\rm flex}$, bending energy $U_{\rm bend}$, and stretching energy $U_{\rm str}$. By integrating the Lennard-Jones potential over the half-space of the substrate and treating the 2D sheet as a continuum [30], the vdW energy can be obtained from the following:

$$U_{\rm vdW}(h) = -\Gamma_0\left[\frac{3}{2}\left(\frac{h_0}{h}\right)^3 - \frac{1}{2}\left(\frac{h_0}{h}\right)^9\right]. \quad (6)$$

Here, the variable h represents the height of the 2D sheet above the substrate, which is a function of position $\vec{r} = (x, y)$ on the sheet, h_0 is the equilibrium distance between graphene and the substrate, which is taken to be 0.6 nm, and Γ_0 is the adhesion energy, here taken to be 0.1 J/m^2 [30]. The bending energy is given by $U_{\text{bend}}(h) = (D/2)[\nabla^2 h(\vec{r})]^2$, where $D = 1.5$ eV is the bending rigidity of graphene [31], while the flexural energy is

$$U_{\text{flex}}(h) = \frac{E}{8(1-\nu^2)}|\nabla h(\vec{r})|^2,$$

where E is Young's modulus and ν is the Poisson ratio [32]. Here, the contribution due to stretching is neglected as the graphene is assumed to be able to slide freely over the surface, owing to its low sliding friction [33].

We then numerically integrate the contributions across the entire surface to attain the total energy $U_{\text{tot}} = \iint dxdy\,[U_{\text{vdw}}(h) + U_{\text{bend}}(h) + U_{\text{flex}}(h)]$, which is discretized into a 100×100 grid. After initializing the height to $h = h_0$ everywhere, we perform an unconstrained minimization of the total energy by varying the graphene-substrate distance at every point using a quasi-Newton algorithm. The resulting graphene height above the surface then allows us to compute the angle of the graphene sheet from the horizontal, i.e.,

$$\sin(\tilde{\theta}) = |\nabla h(\vec{r})| = \sqrt{\left(\frac{dh}{dx}\right)^2 + \left(\frac{dh}{dy}\right)^2},$$

with

$$\theta = \frac{\pi}{2} - \tilde{\theta}.$$

The total FE current from this wrinkled graphene surface is then given by the integral of the $J(F, T, \theta)$ (Eq. (3)) with the angle-dependent supply function [Eq. (2)] obtained from the angle at each point on the surface. We separate the resulting average current density, as shown in Eq. (4), into a field- and temperature-dependent $J(F, T)$ and an angle-dependent term $\langle\cos(\theta)\rangle$ averaged over the whole surface, which is driven by the surface slope given by the ratio $\Delta_{\text{rms}}/L_{\text{cor}}$.

In addition to the local surface slope and its impact on the supply function inside the current density, a sharply curved surface can enhance the electric field near the tips of the tight curves in the surface. This phenomenon, typically referred to as field enhancement, has been noted in several materials including carbon nanotubes (CNTs) [34]. Sharply curved surfaces, such as the hemispherical endcaps of CNTs, can exhibit local electric fields exceeding the applied field $F_M = V/d$ by an enhancement factor γ, so that the field driving FE is given by $F = \gamma F_M$ [35]. The current density at each point on the graphene surface is now a function of both the slope (via the $\cos(\theta)$ term) and the local field (via $F(x, y) = \gamma(x, y)F_M$), so we can write the average current density as

$$J(T, F) = \frac{1}{A}\int J(T, \gamma(x, y)F_M)\cos[\theta(x, y)]dx\,dy. \quad (7)$$

The value of γ can be determined from the radius of curvature and the height of the surface through

$$\gamma \approx \left(\frac{h}{R_C} + a\right)^b,$$

where two of these factors were found to be in the range $a = 1 - 3.5$ and $b \approx 1$ [36]. The tight curvature of a graphene sheet supported on a rough substrate can closely resemble the caps of CNTs, albeit with a smaller height. We calculate the radius of curvature from our surface height from local slope and parabolicity using the standard formula

$$R_C(x, y) = \frac{[1 + \nabla h(x, y)^2]^{3/2}}{|\nabla^2 h(x, y)|}.$$

Then, we use the resulting curvature to compute the enhancement factor

$$\gamma(x, y) = \frac{h(x, y)}{R_C(x, y)} + 1\ ,$$

so that $\gamma = 1$ for a flat surface ($R_C \gg h$).

III. RESULTS AND DISCUSSION

To better understand the trends in FE from graphene, we first calculate the idealized FE current as a function of the applied electric field F and temperature while setting the $\cos(\theta)$ term to 1, which corresponds to a graphene sheet aligned with the electric field. The Dirac-cone band structure of graphene and its nearly linear DOS means that there are few states near the Dirac point, so its carrier (electron and hole) sheet densities are strongly dependent on E_{F} and vice versa through

$$n = \int_0^\infty g(E)f_{\text{FD}}(E, T)dE\ \approx \frac{2}{\pi}\left(\frac{k_B T}{\hbar v_F}\right)^2 \mathcal{F}_1\left(\frac{E_F}{k_B T}\right),$$

where $\mathcal{F}_1$ is the Fermi-Dirac integral of first order [37]. We compute the carrier concentration numerically by integrating the Fermi-Dirac distribution and the DOS obtained from the DFT calculations, resulting in the dependence shown in Fig. 1(a). For holes, the distribution is $1 - f_{\text{FD}}$ and the integrals extend from negative infinity to zero (the Dirac point). In the limit of large sheet density ($E_F \gg k_B T$), the integral simplifies to $\mathcal{F}_1(\eta) \to \eta^2/2$ [38] and $n \approx (1/\pi)(E_F/\hbar v_F)^2$ becomes independent of temperature, as observed on the right-hand side of Fig. 1(a).

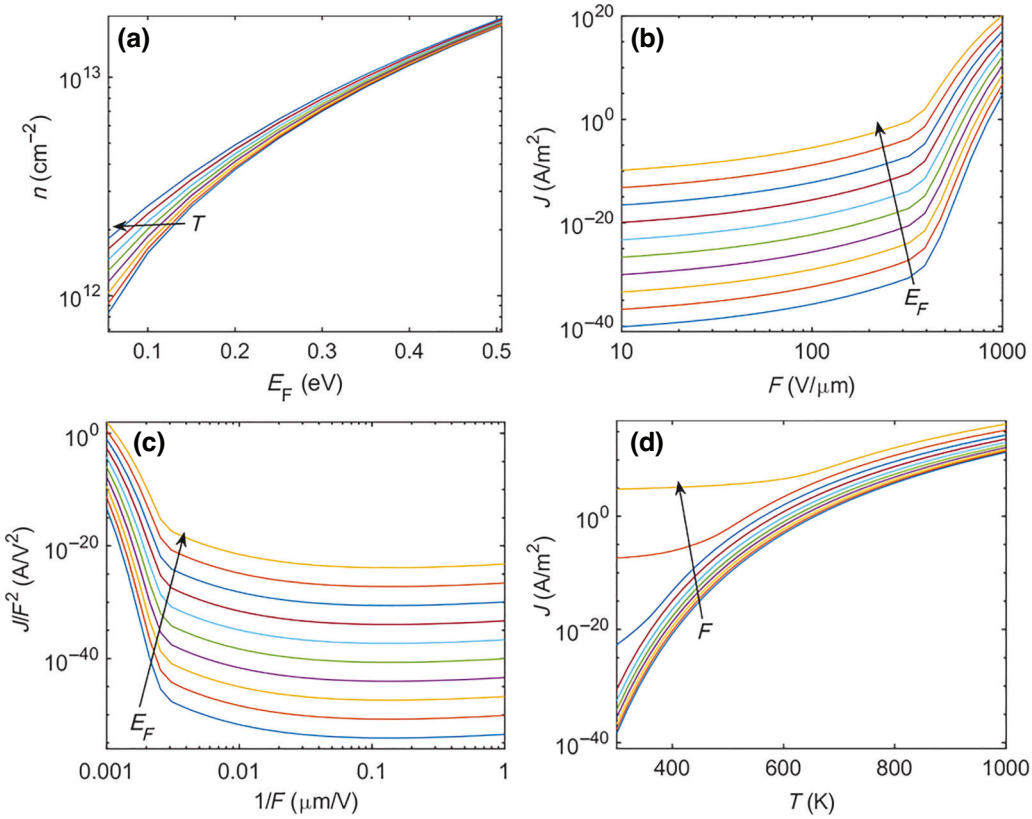

FIG. 1. (a) Sheet carrier density versus Fermi level for temperatures ranging from 300 to 1000 K in increments of 100 K, increasing in the direction indicated by the arrow. (b) Field-emission current density J as a function of electric field F with the Fermi level of graphene varying from 0.1 to 1 eV in increments of 0.1 eV, as indicated by the arrow, showing rapid increase at fields above 300 V/μm. (c) Fowler-Nordheim plot of the FE current density from (b), showing nonlinear behavior typical of two-dimensional materials, with a minimum at fields around 10 V/μm. (d) Plot of current density versus temperature for electric fields varying from 10 to 100 V/μm in increments of 10 V/μm in the direction indicated by the arrow.

On the other hand, the intrinsic concentration is highly dependent on temperature

$$n_i \approx \frac{\pi}{6}\left(\frac{k_B T}{\hbar v_F}\right)^2$$

($\approx 9 \times 10^{10}$ cm^{-2} at room temperature), which, in the opposite limit when T is high and n is low, affects the Fermi level and drives it downward; this trend is indicated by the arrow in Fig. 1(a) where the temperature is varied from 300 to 1000 K.

Being "all surface," graphene is rarely intrinsic. Typical samples have charged impurities trapped between the graphene sheet and the substrate, on the order of 10^{12}–10^{13} cm^{-2} (corresponding to $E_F \approx 0.12$–0.4 eV), which can effectively "dope" the graphene to be n-type [39]. To understand the impact of carrier concentration on FE, we vary the position of the Fermi level E_F relative to the Dirac point. Having $n \gg p$ pushes the Fermi level higher, thereby lowering the effective barrier for emission and significantly increasing the FE current, as we show in Fig. 1(b). The lines correspond to an angle of $\theta = 0$ and $E_F = 0.1, 0.2, \ldots, 1$ eV from right to left, with the highest values exhibiting the lowest threshold field for turn-on. This trend is explained by the rising Fermi level reducing the barrier height relative to the intrinsic graphene's WF (here, $\Phi_{int} = 4.55$ eV), analogous to the effect of barrier lowering in graphene/MoS_2 heterostructures [40]. We also show an FN plot (J/F^2 vs $1/F$) in Fig. 1(c), where we note a minimum around F = 10 V/μm and a deviation from typical FN behavior; this feature has been noted in the literature [11] and attributed to the Dirac-cone band structure [25,41]. Change in the slope on the FN plot may also be partly related to the changes from a linear Dirac-cone electronic structure to a more parabolic structure in higher-lying bands (Fig. S1 in the Supplemental Material [17]), which impacts the relationship between FE current density and field. We also note that the FE current density plot below the change in slope shows a straight line when $\ln(J)$ vs $\sqrt{F}$ (Fig. S2 in the Supplemental Material [17]). However, the analysis of trends for very high fields is beyond the scope of the present work, which is focused on the impact of wrinkling due to a rough substrate on the FE.

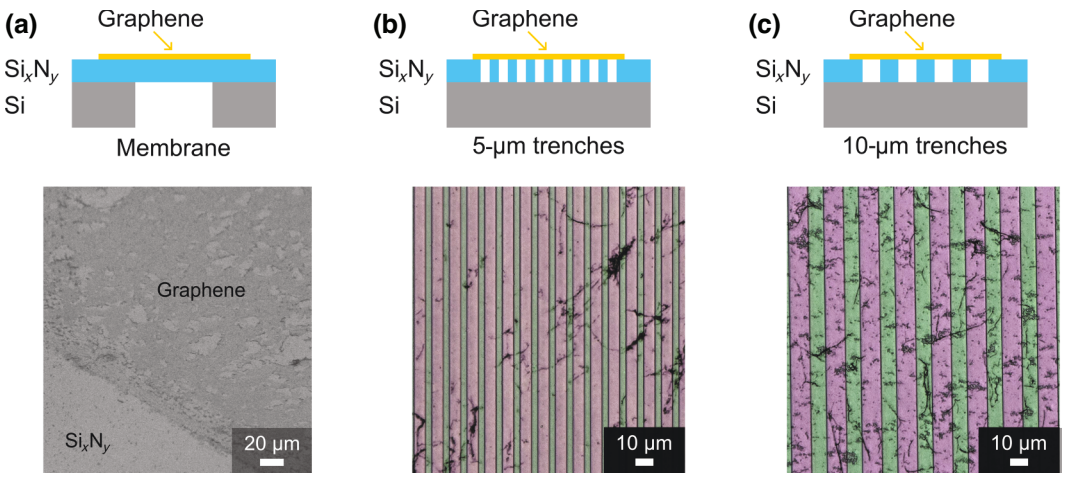

FIG. 2. Monolayer graphene on three different silicon nitride (Si_xN_y) substrates. (a) SEM image of a graphene sheet placed on a 4 mm^2 freestanding Si_xN_y membrane (thickness of 100 nm). The graphene sheets on the (b) 5-μm and (c) 10-μm wide trenches are observed as black structures in the corresponding optical microscopy images.

Next, we turn to the temperature dependence in Fig. 1(d), which can have two contributions. The dominant contribution is from the Fermi-Dirac distribution in the supply function [Eq. (2)], which has an exponentially decaying tail that controls the occupancy of states at a given energy; increasing temperature dramatically increases the occupancy of states near the top of the barrier and boosts the FE current, as we show in Fig. 1(d) where the Fermi level is fixed at 0.1 eV. The second contribution originates from the Fermi level—if the carrier concentration is moderate and fixed externally by charged impurities or, alternatively, by electrostatically gating the graphene, then the Fermi level shifts downward to compensate for the increasing carrier distribution $f_{FD}(E,T)$ with temperature, as shown in Fig. 1(a). We also note the transition between tunneling and thermionic emission, especially at high fields, with F increasing from 30 to 1000 V/μm, as indicated by the arrow in Fig. 1(d). At low fields, the current is driven mostly by temperature; therefore, we can attribute the large variations in FE current at low fields to thermal noise since thermal fluctuations are amplified by the exponential temperature dependence of the thermionic current.

To experimentally explore the predicted trends, we transferred single-crystalline monolayers of graphene onto amorphous silicon nitride (Si_xN_y) substrates and measured FE currents from graphene on macroscopically flat substrates, as shown in Fig. 2(a), and on substrates intentionally patterned with trenches underneath the graphene. The graphene transfer process is described in a previous publication [42]. The trenches have widths of 5 and 10 μm, as shown in Figs. 2(b) and 2(c), respectively. The purpose of the trenches in the substrate is to create regions where graphene is suspended. As a consequence, the angle between graphene and the applied electric field is decreased. Raman measurements confirm that our samples are monolayers of graphene, as evidenced by their 2D peaks (see Supplemental Material, Fig. S3 [17]).

FE currents were measured in our custom-made setup with a 50–125 μm emitter-grid separation and a macroscopic emission area of 36 mm^2. The resulting currents are shown in Fig. 3(a) as a function of the applied vertical electric field, exhibiting the typical exponential onset of FE current when the applied field exceeds the onset field F_M. A Folwer-Nordheim plot of the same data is shown in Fig. S4 of the Supplemental Material [17]. The onset field F_M, defined as the field required for FE current to exceed the background and reach 2×10^{-9} A/m^2, is shown in Fig. 3(b) and ranges from around 15 V/μm in graphene on membranes with no intentional patterning to 23 V/μm in graphene on 5-μm wide trenches, rising to around 27 V/μm when the trenches are 10 μm wide. The decrease in F_M when traversing from wider to narrower trenches is consistent with our model, where the average angle dictates the FE current at a given field because narrower trenches are also more densely spaced, which may lead to larger fractions of the suspended sheet being inclined, particularly near the sidewalls. The angle is further increased by the sidewall adhesion of graphene [43], which tensions the suspended portion of graphene and flattens it, resulting in a low average slope. Therefore, we can expect substrates with narrower trenches to have a larger proportion of vertical sections where graphene adheres to the sidewalls.

However, the tension in suspended graphene has been shown to lead to wrinkling [13], where the wavelength and amplitude of the wrinkles are dictated by a combination of tension, trench width L, and the elastic properties of the substrate in the supported portions. The resulting height profile of the wrinkles is sinusoidal, i.e., $z(x,y) = A\sin(2\pi x/\lambda)$, with x being the direction across the trench,

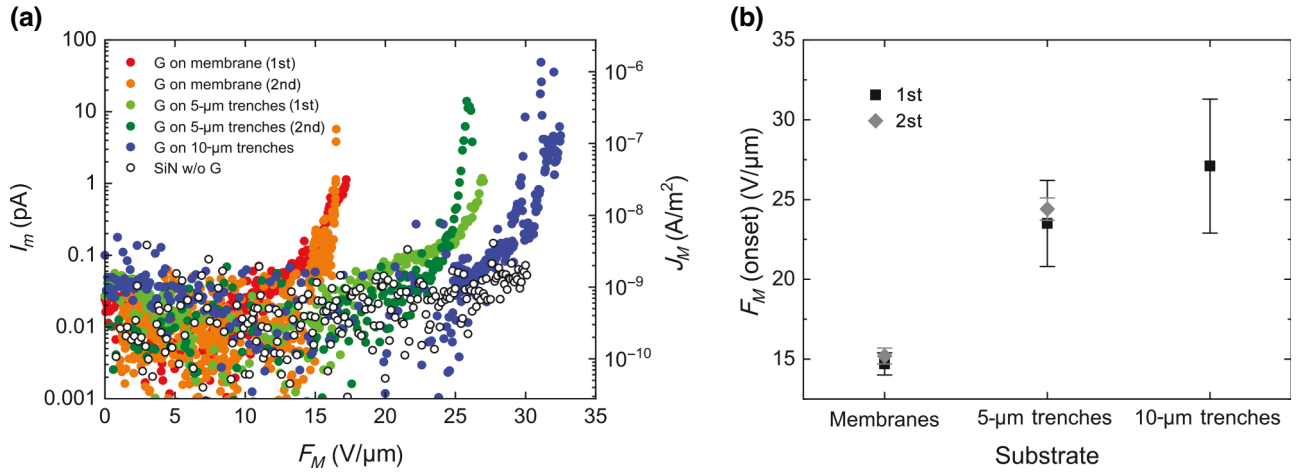

FIG. 3. FE measurements from graphene on different Si_xN_y substrates. (a) Measured current (I_m, left-hand side y-axis) and the macroscopic emission current density (J_M, right-hand side y-axis) dependent on macroscopic applied electric field (F_M) for graphene sheets placed on unstructured Si_xN_y membranes (red and orange dots), on 5-μm wide trenches (green and dark green), and on 10-μm wide trenches (blue). In contrast, no emission current is detected from a pristine silicon nitride substrate without graphene (black circles). Each FE curve shows the mean of the two subsequent measurements. Note that an emitter-grid distance of 50 μm is used, except for the second membrane sample, which is measured with an electrode separation of 125 μm. (b) Macroscopic electric field to allow for FE from the graphene (onset field), which appears to be lower for the unstructured membranes than for the substrates with micrometer-wide trenches.

A as the amplitude, and λ as the wavelength of the wrinkles [44]. The average angle is then related to the slope

$$\frac{dz}{dx} = \frac{A}{\lambda}\cos(2\pi x/\lambda),$$

where wavelength scales with trench width as $\lambda \propto \sqrt{L}$. However, the amplitude is found to scale proportionally to wavelength [45] so that the ratio term A/λ stays constant. We conclude that wrinkling does not impact the average local slope of the surface and, therefore, leaves the FE current unaffected, which, together with sidewall adhesion, explains the relatively small difference in the F_M between $L = 5$ and 10 μm trenches. Counterintuitively, graphene supported on a substrate with no trenches has lower F_M than graphene suspended over trenches [Fig. 3(b)].

To understand why F_M is lower for graphene supported on a substrate without trenches, we analyzed the impact of the corrugation of graphene on a rough substrate on the angle between the graphene sheet and the vertical (direction of electric field). We generated a series of rough surfaces using the procedure described in the Methods section; one example is shown in Fig. 4(a), where a roughness of $\Delta_{rms} = 1$ nm and a correlation length $L_{cor} = 10.5$ nm is used. For this rough surface, we calculated the topology of the graphene sheet on top of it by minimizing the total energy and plotting the resulting angle from the vertical $\cos(\theta)$, as plotted in Fig. 4(b), which reveals local variation around the average value of around 0.2. Increasing surface roughness or decreasing correlation length results in a higher local but also higher average surface slope, which is defined as the ratio of roughness over correlation length, i.e., Δ_{rms}/L_{cor}. The average surface slope of the substrate also increases the slope of the graphene sheet because the graphene largely conforms to the rough substrate surface, resulting in higher $\cos(\theta)$ values, as shown in Fig. 4(c). However, the graphene does not always follow the surface of the substrate exactly and can drape over the sharpest features, causing local delamination if the substrate is too steep [31], resulting in a lower average slope of the graphene than that of the underlying substrate.

Since the total FE current is composed of contributions from the entire surface, which may be corrugated due to conforming to a rough substrate, each segment is weighted by the $\cos(\theta)$ factor. The total FE current will then scale with the average cosine $\langle\cos(\theta)\rangle$ across the entire surface, as shown in Eq. (4). We simulated graphene on rough surfaces while varying roughness from 0 (flat surface) to 2 nm (a typical value for Si_xN_y membranes [46]) and correlation lengths from 2 to 20 nm. Then, we computed the average cosine for each. We kept $\Delta_{rms} < L_{cor}$ because the correlation length is rarely smaller than the roughness, as that would result in surface slope exceeding one and a very steep, fragile surface [47].

The results are plotted in Fig. 4(d), which demonstrate that substrates with large roughness and small correlation length can have as much as 50% of the maximum FE current of a hypothetical vertical sheet that is perfectly aligned with the electric field (as depicted in Fig. 3). On the other hand, large correlation lengths indicate slowly undulating

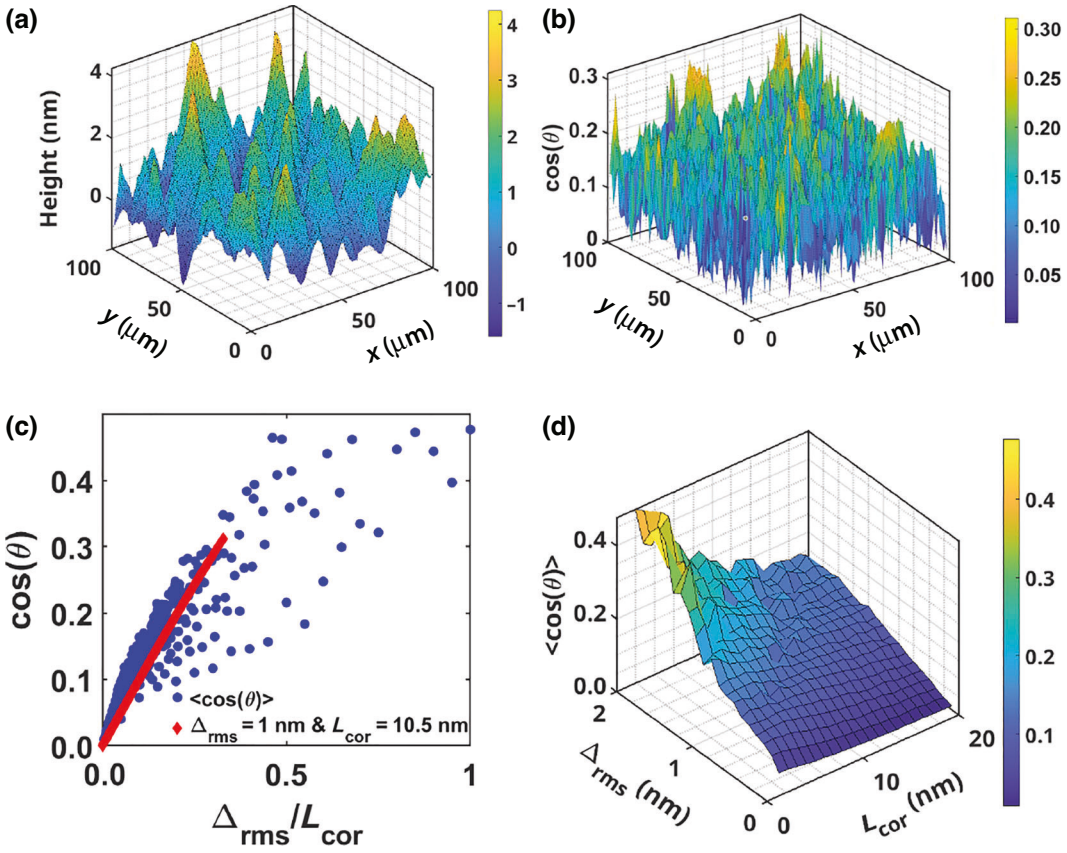

FIG. 4. (a) Topography of the 2D sheet with Δ_{rms} of 1 nm and L_{cor} of 10.5 nm. (b) Cosine of angles as a function of position for the graphene surface plotted in (a), showing large variations in $\cos(\theta)$. (c) Plot of $\cos(\theta)$ for an rms roughness $\Delta_{\mathrm{rms}} = 1$ nm and L_{cor} of 10.5 nm and average $\cos(\theta)$ as a function of the slope. Here, $\cos(\theta)$ is closely related to the average surface slope, given by the ratio $\Delta_{\mathrm{rms}}/L_{\mathrm{cor}}$. (d) Average $\cos(\theta)$ as a function of surface roughness and correlation length, with a maximum value of 0.48. The values of the cosine decrease with decreasing roughness and increasing correlation length.

surfaces. Such surfaces have a very small slope, resulting in less than 10% of the maximum FE current. We can think of our trenches as having large roughness corresponding to their depth, but also very long correlation length corresponding to their width. In this scenario, the average angle is related to the ratio between the two and, thus, it is relatively small compared with the average surface slope of an atomically rough surface $S = \Delta_{\mathrm{rms}}/L_{\mathrm{cor}}$, leading to a lower current. The lower FE current directly results in a higher onset field for FE.

We also examine the curvature of the surface, plotted previously in Fig. 4(a), by plotting its inverse radius of curvature R_C^{-1}, shown in Fig. 5(a). We then repeat the calculation for many combinations of roughness and correlation length to compute the field enhancement factor for each surface. The average of the field enhancement factor of each surface is plotted in Fig. 5(b) against the surface slope, showing that steeper surfaces produce a tighter curvature, resulting in more field enhancement. However, the enhancement factor we calculate for graphene on a rough substrate is modest compared with sharp nanostructures, such as nanowires, nanopillars, or nanocrystals, which have been shown to lead to significantly higher enhancement factors in graphene [15] and related materials such as carbon nanotubes [34].

To compare our calculations more closely with experiments, we plot the current density obtained from the average over the whole surface of the product of the field-dependent and angle-dependent terms [Eq. (7)], as a function of the applied field for a few combinations of roughness and correlation length [Fig. 5(c)]. We then extract the onset field from the point on each curve where the current density crosses 5×10^{-9} A/m^2 and plot the resulting onset field as a function of the inverse of the surface slope, given by the ratio $S^{-1} = L_{\mathrm{cor}}/\Delta_{\mathrm{rms}}$ [Fig. 5(d)]. We observe that the onset field tracks closely with S^{-1} because a larger correlation length or smaller roughness means a flatter surface and, consequently, a lower FE current density, consistent with the trend observed in the experiments. Based on these calculations, onset fields significantly below 10 V/μm could be achievable from graphene on substrates with very atomically rough surfaces, namely, those that have a large roughness and a small correlation length.

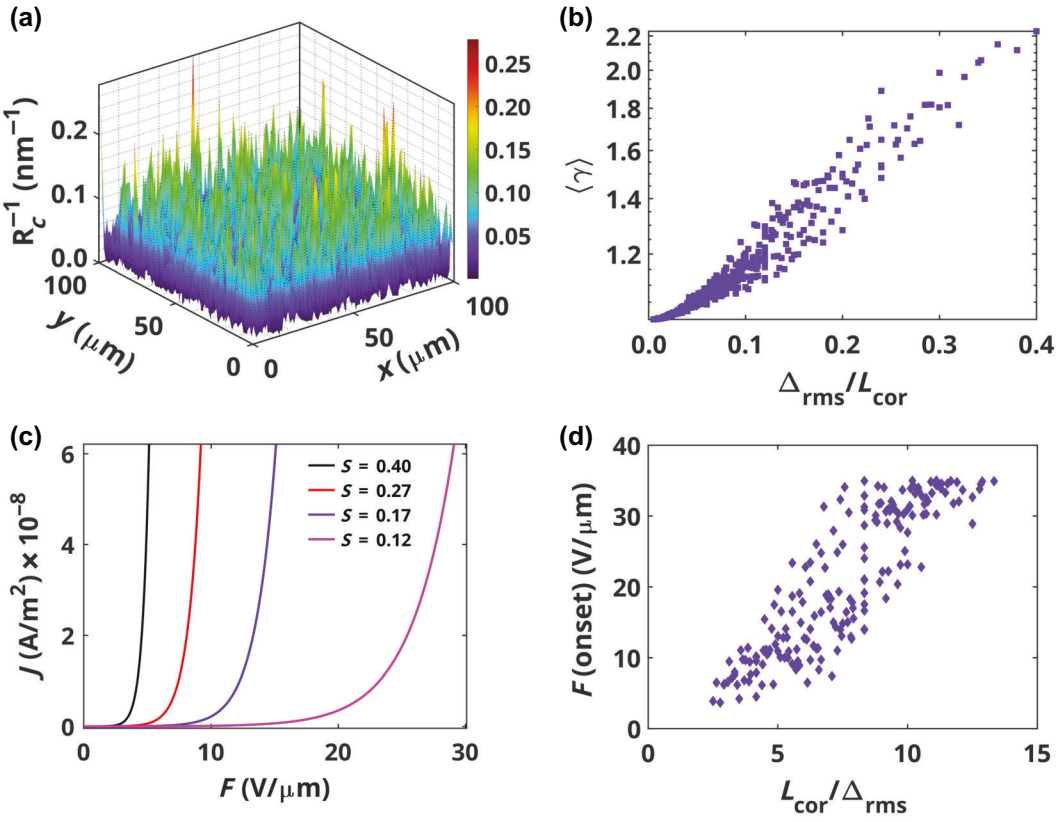

FIG. 5. (a) Surface plot of local surface curvature $R_c{}^{-1}$ for $\Delta_{\rm rms}$ of 1.05 nm and $L_{\rm cor}$ of 12.5 nm, which shows that the local radius of curvature varies across the nanomembrane due to random roughness features. (b) Average field enhancement factor, γ, for each rough surface as a function of its surface slope, which shows that γ increases with increasing surface slope. (c) Field-emission current density J as a function of electric field F at various values of surface slope, $S = 0.40$ ($\Delta_{\rm rms} = 2.00$ nm, $L_{\rm cor} = 5.00$ nm), $S = 0.27$ ($\Delta_{\rm rms} = 1.80$ nm, $L_{\rm cor} = 6.67$ nm), $S = 0.17$ ($\Delta_{\rm rms} = 1.60$ nm, $L_{\rm cor} = 9.17$ nm), and $S = 0.12$ ($\Delta_{\rm rms} = 1.40$ nm, $L_{\rm cor} = 11.67$ nm). (d) Onset electric field (the field needed for the current density to reach 5×10^{-9} A/m^2) as a function of the inverse surface slope. Here, the decrease in the onset field with increasing surface slope implies that a small correlation length and large roughness are ideal for field emission. The calculations use $E_F = 1.0$ eV, which corresponds to a carrier concentration of 7.35×10^{13} cm^{-2}.

IV. CONCLUSIONS

Graphene has potential as a field emitter in a variety of applications owing to its tunable work function, mechanical toughness, and high electrical conductivity. However, it is sensitive to its environment and the substrate on which it is supported. Previous studies established a connection between electron emission and edges or folds in graphene but did not consider the microscopic wrinkling of graphene when supported on atomically rough surfaces. Here, we have studied FE from graphene supported on silicon nitride substrates and suspended over trenches with a width of 5 and 10 μm. We observed a larger FE current and a lower onset field in graphene suspended over the narrower trenches. However, an even higher current and a lower onset field were observed in supported graphene. We developed a comprehensive simulation based on first-principles electronic structure and van der Waals adhesion of graphene to the atomically rough surface of the substrate. We explain that FE depends on the angle between graphene and the electric field, which is dictated by the surface slope of the substrate since graphene largely conforms to it. We found that substrates with larger roughness and lower correlation lengths produce locally steeper surfaces that result in higher FE currents. Our results pave the way toward using substrate roughness as a method for engineering graphene for FE applications.

ACKNOWLEDGMENTS

This material is based upon work supported by the National Science Foundation under Grant No. DMR-2302879 and Deutsche Forschungsgemeinschaft (DFG, German Research Foundation) - project no. 469222030.

[1] C. Lee, X. Wei, J. W. Kysar, and J. Hone, Measurement of the elastic properties and intrinsic strength of monolayer graphene, Science **321**, 385 (2008).

[2] A. H. Castro Neto, F. Guinea, N. M. R. Peres, K. S. Novoselov, and A. K. Geim, The electronic properties of graphene, Rev. Mod. Phys. **81**, 109 (2009).

[3] E. Pop, V. Varshney, and A. K. Roy, Thermal properties of graphene: Fundamentals and applications, MRS Bull. **37**, 1273 (2012).

[4] A. A. Balandin, Thermal properties of graphene and nanostructured carbon materials, Nat. Mater. **10**, 569 (2011).

[5] Y. J. Yu, Y. Zhao, S. Ryu, L. E. Brus, K. S. Kim, and P. Kim, Tuning the graphene work function by electric field effect, Nano Lett. **9**, 3430 (2009).

[6] H. Yuan, S. Chang, I. Bargatin, N. C. Wang, D. C. Riley, H. Wang, J. W. Schwede, J. Provine, E. Pop, Z. X. Shen, *et al.*, Engineering ultra-low work function of graphene, Nano Lett. **15**, 6475 (2015).

[7] F. Zhu, X. Lin, P. Liu, K. Jiang, Y. Wei, Y. Wu, J. Wang, and S. Fan, Heating graphene to incandescence and the measurement of its work function by the thermionic emission method, Nano Res. **7**, 553 (2014).

[8] S. Santandrea, F. Giubileo, V. Grossi, S. Santucci, M. Passacantando, T. Schroeder, G. Lupina, and A. Di Bartolomeo, Field emission from single and few-layer graphene flakes, Appl. Phys. Lett. **98**, 163109 (2011).

[9] Y. Guo and W. Guo, Electronic and field emission properties of wrinkled graphene, J. Phys. Chem. C **117**, 692 (2013).

[10] Z. Xiao, J. She, S. Deng, Z. Tang, Z. Li, J. Lu, and N. Xu, Field electron emission characteristics and physical mechanism of individual single-layer graphene, ACS Nano **4**, 6332 (2010).

[11] Y. S. Ang, S. J. Liang, and L. K. Ang, Theoretical modeling of electron emission from graphene, MRS Bull. **42**, 505 (2017).

[12] W. Wang, X. Qin, N. Xu, and Z. Li, Field electron emission characteristic of graphene, J. Appl. Phys. **109**, 044304 (2011).

[13] S. Deng and V. Berry, Wrinkled, rippled and crumpled graphene: An overview of formation mechanism, electronic properties, and applications, Mater. Today **19**, 197 (2016).

[14] V. Geringer, M. Liebmann, T. Echtermeyer, S. Runte, M. Schmidt, R. Rückamp, M. C. Lemme, and M. Morgenstern, Intrinsic and extrinsic corrugation of monolayer graphene deposited on SiO_2, Phys. Rev. Lett. **102**, 076102 (2009).

[15] L. Iemmo, A. Di Bartolomeo, F. Giubileo, G. Luongo, M. Passacantando, G. Niu, F. Hatami, O. Skibitzki, and T. Schroeder, Graphene enhanced field emission from InP nanocrystals, Nanotechnology **28**, 495705 (2017).

[16] E. L. Murphy and R. H. Good, Thermionic emission, field emission, and the transition region, Phys. Rev. **102**, 1464 (1956).

[17] See Supplemental Material at http://link.aps.org/supplemental/10.1103/PhysRevApplied.22.024022 for measured Raman spectra, calculation of transmission function, electronic structure, and density of states, as well as plots of field emission current versus the square root of the electric field.

[18] S. J. Liang and L. K. Ang, Electron thermionic emission from graphene and a thermionic energy converter, Phys. Rev. Appl. **3**, 014002 (2015).

[19] Y. S. Ang, Y. Chen, C. Tan, and L. K. Ang, Generalized high-energy thermionic electron injection at graphene interface, Phys. Rev. Appl. **12**, 014057 (2019).

[20] P. Giannozzi, S. Baroni, N. Bonini, M. Calandra, R. Car, C. Cavazzoni, D. Ceresoli, G. L. Chiarotti, M. Cococcioni, I. Dabo, *et al.*, Quantum Espresso: A modular and open-source software project for quantum simulations of materials, J. Phys.: Condens.Matter **21**, 395502 (2009).

[21] C. J. Foss and Z. Aksamija, Quantifying thermal boundary conductance of 2D-3D interfaces, 2D Mater. **6**, 025019 (2019).

[22] X. Wei, Q. Chen, and L. Peng, Electron emission from a two-dimensional crystal with atomic thickness, AIP Adv. **3**, 42130 (2013).

[23] M. Zubair, Y. S. Ang, and L. K. Ang, Fractional Fowler-Nordheim Law for field emission from rough surface with nonparabolic energy dispersion, IEEE Trans. Electron Devices **65**, 2089 (2018).

[24] Y. S. Ang, H. Y. Yang, and L. K. Ang, Universal scaling laws in Schottky heterostructures based on two-dimensional materials, Phys. Rev. Lett. **121**, 056802 (2018).

[25] L. K. Ang, Y. S. Ang, and C. H. Lee, Universal model for electron thermal-field emission from two-dimensional semimetals, Phys. Plasmas **30**, 33103 (2023).

[26] V. M. Pereira, A. H. Castro Neto, H. Y. Liang, and L. Mahadevan, Geometry, mechanics, and electronics of singular structures and wrinkles in graphene, Phys. Rev. Lett. **105**, 156603 (2010).

[27] J. H. Seol, I. Jo, A. L. Moore, L. Lindsay, Z. H. Aitken, M. T. Pettes, X. Li, Z. Yao, R. Huang, D. Broido, *et al.*, Two-dimensional phonon transport in supported graphene, Science **328**, 213 (2010).

[28] C. Buran, M. G. Pala, M. Bescond, M. Dubois, and M. Mouis, Three-dimensional real-space simulation of surface roughness in silicon nanowire FETs, IEEE Trans. Electron Devices **56**, 2186 (2009).

[29] A. K. Majee and Z. Aksamija, Electronic transport across extended grain boundaries in graphene, Nano Express **2**, 030007 (2021).

[30] Z. H. Aitken and R. Huang, Effects of mismatch strain and substrate surface corrugation on morphology of supported monolayer graphene, J. Appl. Phys. **107**, 123531 (2010).

[31] T. Li and Z. Zhang, Snap-through instability of graphene on substrates, Nanoscale Res. Lett. **5**, 169 (2010).

[32] F. Ahmadpoor, P. Wang, R. Huang, and P. Sharma, Thermal fluctuations and effective bending stiffness of elastic thin sheets and graphene: A nonlinear analysis, J. Mech. Phys. Solids **107**, 294 (2017).

[33] N. G. Boddeti, R. Long, and M. L. Dunn, Adhesion mechanics of graphene on textured substrates, Int. J. Solids Struct. **97–98**, 56 (2016).

[34] C. P. De Castro, T. A. De Assis, R. Rivelino, F. B. De Mota, C. M. C. De Castilho, and R. G. Forbes, Modeling the field emission enhancement factor for capped carbon nanotubes using the induced electron density, J. Chem. Inf. Model. **60**, 714 (2020).

[35] D. Biswas, A universal formula for the field enhancement factor, Phys. Plasmas **25**, 43113 (2018).
[36] J.-M. Bonard, K. A. Dean, B. F. Coll, and C. Klinke, Field emission of individual carbon nanotubes in the scanning electron microscope, Phys. Rev. Lett. **89**, 197602 (2002).
[37] T. Fang, A. Konar, H. Xing, and D. Jena, Carrier statistics and quantum capacitance of graphene sheets and ribbons, Appl. Phys. Lett. **91**, 0921091 (2007).
[38] A. I. Litvin and S. D. Simonzhenkov, Computation of Fermi-Dirac functions, Comput. Math. Math. Phys. **31**, 100 (1991).
[39] Y. Yin, Z. Cheng, L. Wang, K. Jin, and W. Wang, Graphene, a material for high temperature devices - Intrinsic carrier density, carrier drift velocity, and lattice energy, Sci. Rep. **4**, 1 (2014).
[40] A. Behranginia, P. Yasaei, A. K. Majee, V. K. Sangwan, F. Long, C. J. Foss, T. Foroozan, S. Fuladi, M. R. Hantehzadeh, R. Shahbazian-Yassar, *et al.*, Direct growth of high mobility and low-noise lateral MoS_2–graphene heterostructure electronics, Small **13**, 1604301 (2017).
[41] W. J. Chan, Y. S. Ang, and L. K. Ang, Thermal-field electron emission from three-dimensional Dirac and Weyl semimetals, Phys. Rev. B **104**, 245420 (2021).
[42] T. J. Lyon, J. Sichau, A. Dorn, A. Zurutuza, A. Pesquera, A. Centeno, and R. H. Blick, Upscaling high-quality CVD graphene devices to 100 micron-scale and beyond, Appl. Phys. Lett. **110**, 113502 (2017).
[43] Z. Budrikis and S. Zapperi, Temperature-dependent adhesion of graphene suspended on a trench, Nano Lett. **16**, 387 (2016).
[44] W. Bao, F. Miao, Z. Chen, H. Zhang, W. Jang, C. Dames, and C. N. Lau, Controlled ripple texturing of suspended graphene and ultrathin graphite membranes, Nat. Nanotechnol. **4**, 562 (2009).
[45] E. Cerda and L. Mahadevan, Geometry and physics of wrinkling, Phys. Rev. Lett. **90**, 074302 (2003).
[46] S. R. Hah, C. B. Burk, and T. E. Fischer, Surface quality of tribochemically polished silicon nitride, J. Electrochem. Soc. **146**, 1505 (1999).
[47] B. N. J. Persson, On the fractal dimension of rough surfaces, Tribol. Lett. **54**, 99 (2014).